Extensive test of the three-port quantum mixer theory on 345 GHz superconductor-insulator-superconductor mixers

Honingh, C. E.; Wezelman, J. J.; Dierichs, M. M. T. M. ; de Lange, G.; Schaeffer, H. H. A.; Klapwijk, T. M.; de Graauw, T.

Published in:
Journal of Applied Physics

DOI:
10.1063/1.354347

Publication date:
1993

Extensive test of the three-port quantum mixer theory on 345 GHz superconductor-insulator-superconductor mixers

C. E. Honingh, J. J. Wezelman, M. M. T. M. Dierichs, G. de Lange, H. H. A. Schaeffer, T. M. Klapwijk, and Th. de Graauw

Citation: Journal of Applied Physics **74**, 4762 (1993); doi: 10.1063/1.354347
View online: https://doi.org/10.1063/1.354347
View Table of Contents: http://aip.scitation.org/toc/jap/74/7
Published by the American Institute of Physics

Extensive test of the three-port quantum mixer theory on 345 GHz superconductor-insulator-superconductor mixers

C. E. Honingh and J. J. Wezelman
Space Research Organization of the Netherlands (S.R.O.N.), Landleven 12, 9747 AD Groningen, The Netherlands

M. M. T. M. Dierichs[a] and G. de Lange
Department of Applied Physics and Materials Science Centre, University of Groningen, Nijenborgh 4, 9747 AG Groningen, The Netherlands

H. H. A. Schaeffer
Space Research Organization of the Netherlands (S.R.O.N.), Landleven 12, 9747 AD Groningen, The Netherlands

T. M. Klapwijk
Department of Applied Physics and Materials Science Centre, University of Groningen, Nijenborgh 4, 9747 AG Groningen, The Netherlands

Th. de Graauw
Space Research Organization of the Netherlands (S.R.O.N), Landleven 12, 9747 AD Groningen, The Netherlands

(Received 10 February 1993; accepted for publication 1 April 1993)

Predictions of the three-port model of the quantum theory of mixing are compared with measured results on 345 GHz superconductor-insulator-superconductor waveguide mixers. Single Nb-Al_2O_3-Nb tunnel junctions or two or four identical junctions in series are used as mixing elements. Two different waveguide mixerblocks, one with two tuners and another with one tuner, are used. In addition a single junction with integrated tuning stub is analyzed. Embedding impedances are obtained from fits to the pumped *I-V* curves for all three types of mixing elements. In all cases the dependence of mixer conversion and mixer noise on bias voltage, pump power, and embedding impedance is well described by the three-port model. The measured mixer gain is lower than the calculated gain by a factor of 0.35–0.65, independent of the type of mixer. The use of an additional integrated tuning element does not change this factor. It is concluded that an excess noise power equivalent with a blackbody source of 40–65 K must be added to the mixer noise to account for the absolute value of the observed noise power.

I. INTRODUCTION

The performance of superconductor-insulator-superconductor (SIS) quasiparticle mixers has surpassed that of other techniques for heterodyne detection at submillimeter wavelengths in the frequency range up to 750 GHz.[1–7] This is the result of controlled SIS junction fabrication combined with careful rf design. Nb-Al_2O_3-Nb SIS junctions for heterodyne mixers are now routinely fabricated in several laboratories. High current densities of approximately 10^4 A/cm^2 are achieved, which results in a junction ωRC product of 4–10. R is the junction normal-state resistance, C the junction capacitance, and ω is the local oscillator frequency times 2π. This leads to a demand for small junction areas, between 0.5 and 2 μm^2, to achieve an R between 10 and 100 Ω, which facilitates rf matching problems. Arrays of SIS junctions are frequently used to reduce the demands on junction sizes.

The large ωRC product has the advantage that mixing at harmonic frequencies is much less efficient but it poses considerable matching problems at the design frequency. Waveguide mounts, usually equipped with both a series and a parallel tuner, are generally used. With controlled junction fabrication the larger part of the tuning can be done with superconducting transmission line, fabricated on a chip integrated with the tunnel junctions.[8–10] This development makes the use of planar antennas feasible which, contrary to waveguide mounts, function without any adjustable tuning.[11–13]

Predictions for SIS mixer performance are based on the quantum theory of mixing (QTM), reviewed by Tucker and Feldman.[14] In most cases the three-port approximation is used, which is equivalent to the assumption that all first- and higher-order harmonics are short circuited by the junction's geometrical capacitance. The dependence of mixer gain and mixer noise on the LO power and frequency, the embedding impedances, and the dc *I-V* curve of the junction can be described in relatively simple closed formulas. Low mixer conversion loss, and even conversion gain, together with quantum limited noise behavior are predicted.

Comparison between measured and calculated mixer performance has previously been done at millimeter wave frequencies.[15–17] Agreement is not always found and reported receiver noise temperatures are usually higher than might be expected for quantum limited junction noise per-

[a]Also with Space Research Organization of the Netherlands (S.R.O.N.), Landleven 12, 9747 AD Groningen, The Netherlands.

 0021-8979/93/74(7)/4762/12/$6.00

formance. Knowledge of the embedding impedances at all relevant frequencies is essential to compare mixer performance to the quantum theory of mixing. Some of the reported differences between theory and measurements are probably due to insufficient knowledge of the embedding impedances,[15] but even in cases where the embedding impedance is well known, theory and measurements do not always agree. Quantum limited noise performance has been demonstrated at 100 GHz.[9,10,16] In the comparison with theory by Mears *et al.*[16] the measured mixer gain as a function of backshort position is approximately 2 dB lower than calculated. The influence of the quality of the unpumped dc *I-V* curve has been emphasized by McGrath *et al.*[15] These authors report that theory and experiment deviate when the width of the current rise at the gap in the dc *I-V* curve is smaller than the voltage equivalent to one photon. At submillimeter wavelengths this condition is always fulfilled.

As has been argued at an early stage of SIS mixer development, a number of junctions in series alleviates the restrictions on the size of the junctions compared to those for a single junction,[18,19] without degrading the mixer performance. Using various arrays of junctions, however, Crété *et al.*[20] find an unexplained amount of excess noise. Feldman *et al.*,[17] on the other hand, report good agreement between measured and calculated mixer gain for an array of 13 elements in series and Pan *et al.*[9] demonstrate a well-understood noise performance at 115 GHz using a two-junction in-series array.

In an earlier article we reported measurements at 350 GHz on one specific mixer element consisting of two $Nb/Al_2O_3/Nb$ junctions in series measured in a two-tuner waveguide block.[21] A systematic difference between measured and calculated results was found which appeared to be independent of the mixer bias parameters. In this article we report on an extension of those measurements to other samples also using single junctions and four junctions in series. Measurements on a total of six different samples are described. We used the same mixerblock as described in Ref. 21 with two tuners but also a similar mixerblock with only one tuner. In addition, one of the samples has an integrated tuned junction. Receiver noise temperatures between 110 and 160 K, which are comparable with results found elsewhere, have been obtained for all samples.

The organization of the article is as follows: In Sec. II we briefly summarize our experimental setup. The various contributions to the i.f. output are analyzed in Sec. III and integrated with predictions of the three-port mixer model in Sec. IV, together with experimentally determined embedding impedances. The numerical values of the system components are determined in Sec. V, followed by the junction characteristics in Sec. VI. The detailed comparison of experiment and theory is carried out in Sec. VII. In Sec. VIII various possible causes for the differences between theory and experiments are discussed.

II. MEASUREMENT SETUP

The mixer is part of the receiver arrangement shown in Fig. 1. Input signal and local oscillator power are combined by a beamsplitter (I), made of mylar or Kapton® sheets of various thicknesses. As a signal source we use an Eccosorb® blackbody at two different temperatures, room temperature and liquid-nitrogen temperature. The local oscillator signal is generated by a carcinotron or a solid-state oscillator.

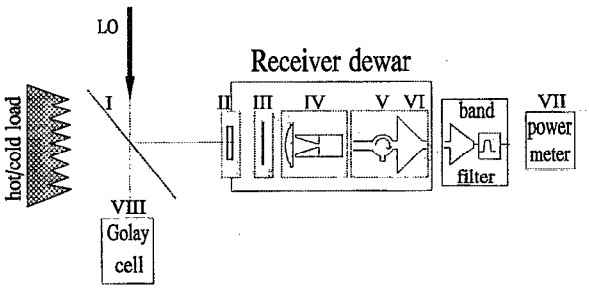

FIG. 1. Diagram of the receiver. I is the beamsplitter and II is the mylar vacuum window. Units III, IV, V, and VI are located inside the liquid-helium Dewar. III is the IR filter at 77 K, IV is the mixer, with lens-horn combination included. V is the isolator at the i.f. frequency and VI is the cooled HEMT i.f. amplifier. VII is the calibrated i.f. power meter and VIII is the Golay cell that registers the LO power.

The signal and local oscillator beam pass through a 250-μm-thick vacuum window (II) of mylar and a resonant quartz IR filter (III), with a thickness of 230 μm at 77 K. A cold (5–8 K) lens focuses the beam on the horn of the mixerblock. The mixer block (IV) is bolted the a cold plate of the Dewar at a temperature of approximately 4.5 K. We use a diagonal horn[22] which is joined to the waveguide by a simple smooth transition. Measurements at IRAM[23] and by Johanson and Whyborn[24] confirm that the chosen transition does not degrade the performance of the horn. It has been verified that the mixer beam couples fully to the blackbody source, and also that the side lobes are down at least -15 dB.

Two similar waveguide mixer blocks have been used. One block with two tuners (2T), an *E*-plane tuner and a backshort, has been described elsewhere.[25] In the other block (1T) the *E*-plane tuner is absent. The waveguides of both blocks have the same dimensions, 625×150 μm^2, and both blocks are made of oxygen-free high-conductivity (OFHC) copper. As tuners we use in both cases adjustable noncontacting shorts. Block 1T has an integrated horn whereas in block 2T the horn is bolted to the block. Both horns have the same dimensions and the same lens is used for both blocks. The dc Josephson effect is suppressed by a magnetic field generated by a superconducting coil with its axis parallel to the plane of the junction.

The SIS junctions with integrated rf filters, fabricated on a fused quartz substrate, are glued in a substrate channel across the waveguide. The plane of the junction is in parallel with the narrow wall of the waveguide. In both blocks the substrate channel is 190×210 μm^2, and the substrate thickness is 90–95 μm.

The i.f. frequency is coupled to the i.f. chain through a spring contact perpendicular on the substrate. In some of the measurements with block 2T we have used a 500–50 Ω matching transformer at the intermediate frequency (i.f.),

with a bandwidth of 200 MHz. The dc bias is applied through a commercial bias T. Between the mixer and the first i.f. amplifier (VI) we use an isolator (V) to avoid standing waves due to possible mismatch. The first amplifier is a 4.5 K cooled HEMT amplifier (Berkshire Technologies) with a specified gain of 40 dB (1.2–1.7 GHz) and a noise temperature of 2 K. Outside the dewar the i.f. output power is further amplified to a level between 1 and 50 μW.

The i.f. output power and the dc current through the junction are measured simultaneously. The i.f. output power is in most cases measured in two different overlapping bandwidths of 80 and 240 MHz. The 80 MHz band is measured with a calibrated power meter (VII) and the 240 MHz band with a (fast) diode detector. The LO power transmitted by the beamsplitter is registered with a Golay cell (VIII).

III. ANALYSIS OF THE i.f. OUTPUT POWER

The central conclusion of this article is that the i.f. output power of the receiver, including all possible contributions, is given by the following equation:

$$P_{\text{out}}(V,V_\omega)=A_{\text{i.f.}}[A_m(V,V_\omega)A_{\text{ex}}P_{\text{in}}+A_m(V,V_\omega)P_{\text{ex}} +P_S(V,V_\omega)+P_Q(V,V_\omega)+P_{\text{i.f.}}(V,V_\omega)]. \tag{1}$$

The equation is a function of the dc bias voltage V and the rf voltage V_ω over the mixing element. P_{in} is the signal incident on the mixerblock (IV in Fig. 1) and $A_{\text{i.f.}}$ is the gain of the i.f. system, both determined from separate measurements and calculations.

In the first two terms the parameters A_{ex} and P_{ex} are introduced to account for the deviations between calculations and experiment. $A_m(V,V_\omega)$ in these terms is the mixer gain as calculated from the quantum theory of mixing. The experimental mixer gain is determined from the subtraction of the i.f. output power levels measured for two different values of P_{in}. Assuming that all other terms in Eq. (1), including the terms with P_{ex}, do not change with different P_{in}, and assuming that the mixer is linear, A_{ex} is determined. If theory and measurement would agree completely A_{ex} would be 1.

As is shown (Sec. IV) an additional constant input power P_{ex} multiplied by the mixer gain must be added to Eq. (1). The value of P_{ex} would be zero in the case of a complete correspondence between theory and measurement. If we use a value $P'_{\text{ex}}=P_{\text{ex}}/A_{\text{ex}}$ and place P'_{ex} together with P_{in} within brackets in the first term of Eq. (1), mathematically the same result is obtained. As we argue in Sec. VIII A, we believe that the experimental results justify the definition chosen in Eq. (1).

The part of Eq. (1) that is calculated directly from the quantum theory of mixing consists of two terms, $P_S(V,V_\omega)$ and $P_Q(V,V_\omega)$. $P_S(V,V_\omega)$ represents the thermal noise power and the shot-noise power generated by fluctuations in the tunnel current. $P_Q(V,V_\omega)$ is due to the vacuum fluctuations in the photon bath. Both terms and $A_m(V,V_\omega)$ are calculated from the measured unpumped I-V curve and the embedding impedances as determined from the pumped I-V curve.

The last term in Eq. (1) gives the contribution of the i.f. stage of the receiver:

$$P_{\text{i.f.}}(V,V_\omega)=kB[T_{\text{isol}}|\Gamma_{\text{i.f.}}(V,V_\omega)|^2+T_{\text{i.f.}}]. \tag{2}$$

$T_{\text{i.f.}}$ is the noise temperature of the amplifier and B is the bandwidth of the i.f. system. The first term gives the thermal noise power reflected from the i.f. port of the mixer. $\Gamma_{\text{i.f.}}(V)$ is the bias-voltage-dependent voltage reflection coefficient due to the mismatch between $\text{Re}(Y_L)$ and $dI_{\text{dc}}(V)/dV$. Like P_{in} and $A_{\text{i.f.}}$, $P_{\text{i.f.}}$ is determined in separate measurements.

IV. APPLICATION OF THE THREE-PORT MIXER MODEL

The performance of the mixer is to a large extent determined by the electromagnetic environment of the junction. To calculate the mixer gain A_m, the noise contributions from the junction P_S, and the photon field P_Q, the three-port mixer model is used together with experimentally determined embedding impedances.

A. Definition of A_m, P_S, and P_Q

The mixer gain and noise are calculated from the quantum theory of mixing.[1] The three-port approximation is used which means that the currents generated at the first harmonic and higher harmonics are assumed to be short circuited by the junction's geometrical capacitance.

To calculate the mixer performance the small signal voltages v_i present across the junction at the three relevant frequencies, f_{usb} ($i=1$), $f_{\text{i.f.}}$ ($i=0$), and f_{lsb} ($i=-1$), are taken to be the response to three current generators i_j. The current generators represent the incoming signal at each of these frequencies. Small signal currents and voltages are linearly related by the 3×3 conversion matrix Z_{ij}, $v_i=Z_{ij}i_j$, taken from Tucker and Feldman,[14]

$$Z_{ij}=\begin{pmatrix} Y_{11}+Y_{\text{usb}} & Y_{10} & Y_{1-1} \\ Y_{01} & Y_{00}+Y_L & Y_{0-1} \\ Y_{-11} & Y_{-10} & Y_{-1-1}+Y_{\text{lsb}} \end{pmatrix}^{-1}, \quad i,j=1,-1. \tag{3}$$

The Y_{ij} elements characterize the junction array at a certain bias condition, determined by the LO power and the LO frequency, the embedding impedances, and the dc bias voltage.

The terms added to the diagonal elements of the matrix are the terminating admittances at the upper sideband ($Y_{\text{usb}}=G_{\text{usb}}+iB_{\text{usb}}$), the intermediate ($Y_L=G_L$) frequency, and the lower sideband ($Y_{\text{lsb}}=G_{\text{lsb}}+iB_{\text{lsb}}$) input port of the mixer. The impedances are determined with a fitting procedure outlined in the following subsection.

Using Eq. (3) the gain of the mixer is given by

$$A_m(V,V_\omega)=4G_L[G_{\text{usb}}|Z_{01}(V,V_\omega)|^2 +G_{\text{lsb}}|Z_{0-1}(V,V_\omega)|^2]. \tag{4}$$

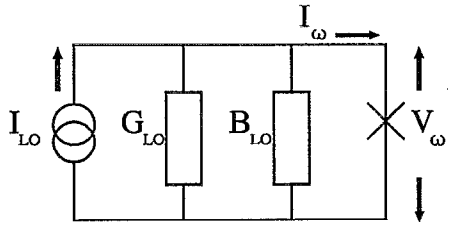

FIG. 2. The Norton equivalent of the embedding circuit and the SIS array. $G_{LO}+iB_{LO}$ is the embedding admittance and I_{LO} represents the LO input power. I_ω and V_ω are the rf current and voltage at the junction (array), depicted by a cross.

Part of the noise in the mixer, $P_S(V,V_\omega)$, is generated by fluctuations in the tunneling current resulting from the combination of bias voltage and LO power. The rms expectation value of this current fluctuation is calculated using the current correlation H-matrix formulation derived in Ref. 14. The noise output power to an i.f. load admittance G_L is given by

$$P_S(V,V_\omega)=G_L B \sum_{i=-1}^{1}\sum_{j=-1}^{1} Z_{0i}(V)Z_{0j}^{*}(V)H_{ij}(V), \quad i,j=-1,1, \tag{5}$$

where B is the bandwidth of the i.f. system. Z_{0j}^{*} denotes the conjugate of Z_{0j}. We apply this analysis to single junctions and arrays of two and four junctions in series. In doing that we will assume that the shot-noise contributions from junctions in series are uncorrellated.[26,27] The contribution of the vacuum fluctuations, $P_Q(V,V_\omega)$, as calculated by Wengler and Woody[28] by quantizing the incident radiation field, is added to the shot noise. It is given by

$$P_Q(V,V_\omega)=B\sum_{i=-1}^{1}(A_m)_{0i}(V,V_\omega)\frac{1}{2}hf_i\coth\left(\frac{hf_i}{2kT_i}\right), \tag{6}$$

where $(A_m)_{0i}$ is the mixer conversion from frequency f_i to the i.f., k is Boltzmann's constant, and T_i is the temperature of the equilibrium photon bath at f_i. For temperatures around 4.5 K the hyperbolic cotangent is approximately 1.

B. Determination of the embedding impedances

The embedding impedances of the actual mixer are determined from the measured pumped I-V curve. Two parameters are used to characterize the embedding circuit. A third parameter is used for the incident LO power. G_{LO} and B_{LO} are the real and imaginary part of the total embedding impedance Y_{LO} at the LO frequency and $|I_{LO}|$ is the absolute value of a complex current source representing the incident LO power (Fig. 2). To accurately relate the pumped I-V curves with theoretical curves various strategies have been used in the past. We have used the computerized voltage match method first introduced by Skalare.[29]

The rf voltage V_ω is calculated from Eq. (7) at every bias point by comparing the pumped I-V curve, $I_{p_{dc}}(V,V_\omega)$, with the unpumped I-V curve, $I_{dc}(V)$, measured under the same conditions

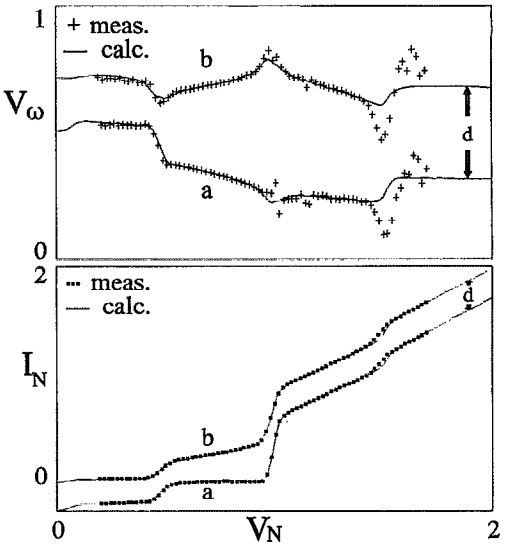

FIG. 3. Measured (+,■) and calculated (−) rf voltage V_ω and dc current I_N of a two-junction array as a function of bias voltage V_N. The bias voltage is normalized to two times the gap voltage, $4\Delta/e$, and the bias current to $4\Delta/e$ divided by the normal-state resistance of the array, leading to a normalized resistance of 1. The curves (a) are vertically displaced by a distance d for clarity. The values for Y_{emb}, normalized to $\frac{1}{110}\ \Omega$, are $1.66-0.33i$ for curves (a) and $0.99+2.15i$ for curves (b).

$$I_{p_{dc}}(V,V_\omega)=\sum_{n=-\infty}^{n=\infty}J_n^2\left(\frac{eV_\omega}{hf_{LO}}\right)I_{dc}\left(V+n\frac{hf_{LO}}{e}\right). \tag{7}$$

e is the electron charge, h is Planck's constant, and f_{LO} is the local oscillator frequency. J_n is the Bessel function of the order n. Knowing $V_\omega(V)$, the in-phase, $I_\omega(V,V_\omega)$, and out-of-phase, $I'_\omega(V,V_\omega)$, rf current through the junctions can be calculated from the expressions given in Ref. 14.

These quantities are related through the network theorem (Fig. 2):

$$|I_{LO}|^2=[I_\omega(V,V_\omega)+G_{LO}V_\omega(V)]^2+[I'_\omega(V,V_\omega)+B_{LO}V_\omega(V)]^2. \tag{8}$$

Using the fact that Eq. (8) must hold for all bias points G_{LO}, B_{LO}, and $|I_{LO}|$ are determined. For the fitting procedure we select mainly bias points on the first and second photon step below the gap voltage because the first deviations from the theory, presumably due to heating, occur above the gap voltage. Arrays of junctions in series are treated as a single effective junction.

In Fig. 3 an optimum calculated I-V curve is compared with a measured I-V curve for an arbitrary value of pump power for two different embedding circuits. The excellent agreement between theory and experiment for V_ω, especially below the gap voltage, provides very reliable values of the embedding impedances. Fits of comparable quality are reached for all relevant frequencies and for most pump powers. Deviations are found mainly at high power levels and they appear first above the energy gap.

At bad coupling conditions high power levels are needed to get a well-developed pump step and a decrease of the gap is observed which depends on the dc current

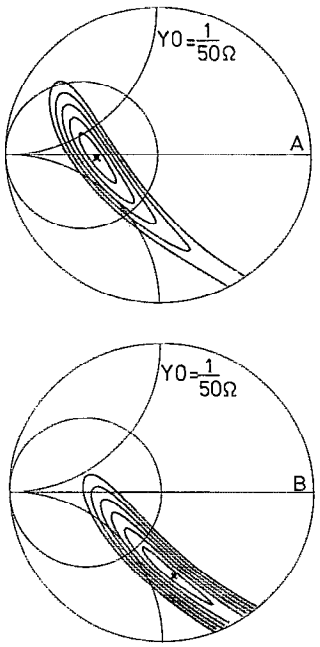

FIG. 4. Smith chart with error contour plots corresponding to the fitted embedding admittances (A) $1.9+0.1i$ and (B) $0.8+0.8i$. In arbitrary units the innermost contour of (A) is 0.03 and of (B) is 0.02. The spacing between the contours is 0.01.

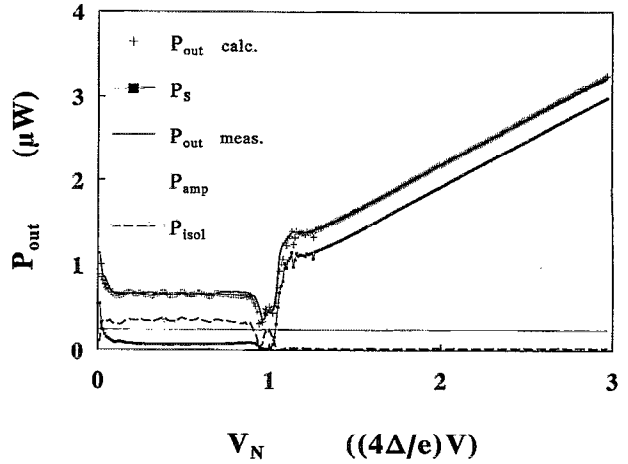

FIG. 5. i.f. output power of the unpumped junction array S44-e11, as a function of bias voltage, measured (solid line) and calculated (+). The various contributions to the i.f. power are the shot noise and thermal noise P_S (■), the thermal noise reflected at the i.f. port of the mixer $P_{\rm isol}$ (dashed line), and the constant contribution of the i.f. amplifier $P_{\rm i.f.}$ (thin continuous line).

through the junction. For high-quality fits the whole bias region below the gap is needed. Therefore, we restrict this analysis to the sensitive tuning range of the mixer, where the LO power is low.

We have repeated fittings and measurements at the same point several times to determine the variations in the values of the admittances. The estimated value of $B_{\rm LO}$ did not vary by more than $\pm 10\%$ between different fits. For a more capacitive embedding circuit the values for $G_{\rm LO}$ and $|I_{\rm LO}|$, which are directly related through the pump power, can vary by up to a factor of 2. Typical error contour plots are given in Fig. 4 both for a capacitive and an inductive embedding. Because the relative input pump power is measured, pumped I-V curves at different embedding impedances but at the same power level can be related. This provides an extra constraint for $G_{\rm LO}$ and $|I_{\rm LO}|$ which improves the accuracy of the fitted embedding impedance to an error of about $\pm 20\%$ in $G_{\rm LO}$. As shown previously[21] these impedances agree well with those found in a scale design model.

The imaginary part of the i.f. load admittance is negligible between 1 and 2 GHz, as has been determined by a separate reflection measurement at the i.f. port of the mixer with a standard network analyzer. A low input power (−65 dB) is used to prevent a change in the dynamic impedance of the junction at the i.f. frequency. In the calculations we use $Y_L=G_L=(50\ \Omega)^{-1}$.

V. CHARACTERIZATION OF THE SYSTEM

To accurately determine the contribution of the various parts of the receiver to the measured i.f. output noise power [Eq. (1)], the contributions of the i.f. chain and of the input losses are determined from separate measurements and calculations.

The i.f. output power of the receiver without applied LO power is given by Eq. (1), with $A_m=0$. The contribution of $P_Q(V,0)$ reduces to the small value of about one photon at the i.f. frequency [Eq. (6)], which is further neglected. The shot-noise output power of the junction, P_S as given in Eq. (5), becomes for $V_\omega=0$ (Ref. 30)

$$P_S(V,0)=\frac{2eB}{N}G_L I_{\rm dc}(V)\coth\left(\frac{eV}{2kT}\right)\left(\frac{dI_{\rm dc}(V)}{dV}+G_L\right)^{-2}. \tag{9}$$

$I_{\rm dc}(V)$ is the dc I-V characteristic of the array at the physical temperature T, G_L is the load impedance of the i.f. system, and N is the number of junctions in series, treated as N uncorrellated noise sources.[21,25] With these definitions the gain $A_{\rm i.f.}$ and noise $P_{\rm i.f.}$ of the i.f. system follow from a comparison of Eq. (1) with the measured i.f. output power for an unpumped junction.

A typical registration of the i.f. output power as a function of bias voltage is given in Fig. 5 (solid line). As expected the curve is unchanged under application of a hot or a cold load signal. The curve indicated with plus signs is the theoretical result of Eq. (1). For $A_{\rm i.f.}=38.7$ dB, $T_{\rm i.f.}=3$ K, and $T_{\rm isol}=4.5$ K excellent agreement is obtained. The total noise power consists of a shot-noise contribution (P_S, solid squares) and two contributions from the i.f. chain. $P_{\rm amp}$ (thin line) is the noise contribution of the i.f. amplifier, independent of bias voltage. $P_{\rm isol}$ (dashed line) is the thermal noise contribution of the isolator which is dependent on the bias voltage.

The gain $A_{\rm i.f.}$ is determined with an accuracy of ± 0.2 dB from the slope of the curve above two times the gap voltage. A gain of 38.7 dB is in good agreement with values measured directly with a network analyzer. For the differ-

TABLE I. Parameters of tested devices and mixers. N is the number of junctions in series, G and B are the real and the imaginary part of the embedding admittance at the LO frequency (LO), the upper sideband frequency (usb), and the lower sideband frequency (lsb). The embedding admittance is normalized to the normal-state conductance of the corresponding junction array $1/R_n$. I_{LO} is a measure for the incident LO power $[I_{LO}^2/8G_{LO}$ in units of $(NV_{gap})^2/R_n]$, with $V_{gap}=2.8$ mV. A_{ex} and P_{ex} are the fitting parameters [Eq. (1)] required to match theory to data. MB denotes type of mixer block. 1T stands for one backshort, and 2T for the block which has an additional E-plane tuner. The asterisk indicates the use of a 500–50 Ω i.f. transformer, and a plus sign indicates the use of an integrated tuning element. T_{res} is the DSB receiver noise temperature referred to the input of the receiver Dewar, and is calculated using Planck's law.

No.	N	G_{LO}	B_{LO}	G_{usb}	B_{usb}	G_{lsb}	B_{lsb}	I_{LO}	A_{ex}	P_{ex} (K)	MB	T_{rec} (K)	Sample
1	1	1.2	0.34	0.9	0.7	2.2	−0.1	1.15	0.43	49	1T	170	S44-f1
2	1	1.4	1.19	1.7	1.3	2	1.2	1.36	0.38	46	2T	185	S44-f1
3	1	1.5	0.35	1	0.6	2.4	0.9	1.28	0.35	48	2T	200	S44-f1
4	1	0.6	0.84	0.4	2.5	1.7	0.14	1.07	0.39	51	2T	260	S44-f1
5	1	1.2	0.4	0.8	0.76	1.6	0.27	1.27	0.4	47	2T*	165	S44-f1
6	1	0.5	0.25	0.5	0.38	0.5	0.16	0.79	0.58	63	1T+	157	S42-f4
7	2	1.8	0.52	0.5	0.88	2.7	0.52	1.25	0.57	41	2T*	130	S234
8	2	0.8	1.1	0.6	1.33	1.8	0.84	1.09	0.5	41	2T*	155	S234
9	2	1	0.04	1.1	0.44	1.1	−0.6	1.41	0.5	62	1T	180	S44-e6
10	2	1	0.04	1.1	0.44	1.1	−0.6	1.02	0.47	58	1T	190	S44-e6
11	2	1.5	1.16	1.1	1.4	2.5	0.97	0.98	0.61	53	1T	157	S44-e11
12	2	1.5	1.16	1.1	1.4	2.5	0.97	1.22	0.63	53	1T	148	S44-e11
13	2	1.5	1.16	1.1	1.4	2.5	0.97	1.43	0.65	53	1T	140	S44-e11
14	4	1.3	0.5	1.3	0.8	2.2	0.2	1.4	0.48	45	2T	150	S44-c3
15	4	1.3	0.5	1.3	0.8	2.2	0.2	1.12	0.44	45	2T	170	S44-c3

ent samples reported here the same value is found within the given accuracy. The noise temperature of the amplifier $T_{i.f.}$ and the isolator T_{isol} can be separated easily due to the bias-voltage dependence of $\Gamma_{i.f.}(V)$. $T_{i.f.}$ is slightly higher than the manufacturer specified (3 ± 0.5 K) and for T_{isol} we find 4.5 K. If we use an i.f. transformer we find $T_{isol}=5.5$ K, possibly due to a detoriated isolator performance.

The input power on the mixer P_{in}, follows from the load at a specific temperature by taking into account the transmission coefficients of the input optics:

$$P_{in}=P_{load}A_{bs}A_wA_f+P_{bs}(1-A_{bs})A_wA_f$$
$$+P_w(1-A_w)A_f+P_f(1-A_f). \quad (10)$$

The transmission coefficients are beam splitter (I in Fig. 1): $A_{bs}=89\%\pm1\%$, Dewar window (II): $A_w=95\%\pm1\%$, and IR filter (III): A_f is $95\%\pm1\%$. The values for the power (P_{load}, P_{bs}, P_w, and P_f) are determined from Planck's law in a bandwidth B. For the load we use the temperatures 295 and 77 K. It is estimated that the Dewar window has a temperature of 285 K and the rf filter has a temperature of 80 K. With the given values the effective input temperatures on the mixer block due to the hot and the cold load are 275 and 101 K, respectively. Note that the lens/horn combination is taken as part of the mixer block.

VI. JUNCTION CHARACTERISTICS

The $Nb/Al_2O_3/Nb$ SIS junctions used are fabricated on fused quartz substrates using the trilayer approach first introduced by Gurvitch, Washington, and Huggins.[31] Junctions are patterned with optical lithography. Details of the fabrication are given by Dierichs *et al.*[32] The six samples are taken from three different fabrication batches, indicated in Table I as S44, S42, and S234. The dc I-V curves of the samples are given in Fig. 6. Two samples have a single-junction mixing element, three samples two junctions in series, and one sample is four junctions in series. The single-junction sample S42 contains an open-circuited integrated tuning stub of 115 μm, which resonates the junction capacitance at approximately 335 GHz. The area of the junctions varies from 0.6 to 2.2 μm^2, and the ωRC product lies between 4.5 and 6.5 for all samples. The normal-state resistance of the junctions varies from 27 to 54 Ω per junction. The sample with four junctions in series represents almost exactly the same effective junction as the

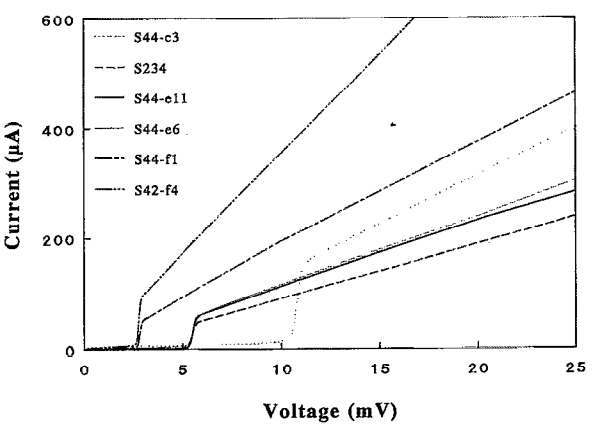

FIG. 6. Unpumped I-V curves of the samples used in this article S234, S42, and S44 are the different fabrication batches. The photolithographically defined areas of the two single-junction elements are 0.6 and 1 μm^2, of the two in-series elements 1 μm^2 for each junction and for the four in-series array 2 μm^2 per junction. A magnetic field is applied to suppress the Josephson current.

single-junction sample S44. Both samples are part of the same batch and have the same ωRC product.

A magnetic field of about 300 G is applied to cancel the supercurrent. This field is strong enough to reach the second minimum in the Fraunhofer diffraction pattern. At higher fields, beyond approximately 400 G, the onset of the current rise at the gap moves to lower bias voltages, indicating a smearing of the density of states by the magnetic field.

VII. MIXER PERFORMANCE

The receiver noise temperature at the optimum bias voltage T_{rec} is given in Table I for each sample. T_{rec} is determined from the ratio of the i.f. output power at a hot (295 K) and cold (77 K) input load and is referred to the input of the receiver Dewar. The input power from the load is, as elsewhere in the analysis, calculated using Planck's law. The receiver noise temperature in the Rayleigh–Jeans limit, which is commonly used in the literature, is obtained by subtracting approximately 15 K from T_{rec}.

A typical example of the i.f. output power, as a function of bias voltage, is given by the lines in Fig. 7(a), subsequently with a 295 and a 77 K blackbody source as input. The measurements reported here have mainly been done at a LO frequency of 352 GHz. The pumped I-V curve, measured simultaneously with the i.f. signal, is used to obtain the embedding impedance at the LO frequency, given in Table I. The LO frequency is tuned 1.4 GHz upward and downward, and pumped curves at the two sideband frequencies are measured to determine Y_{usb} and Y_{lsb}, also shown in Table I.

Given these embedding impedances and assuming $A_{ex}=1$ and $P_{ex}=0$, the i.f. output power is calculated from Eq. (1). The result is shown in Fig. 7(a) by ● for a hot 295 K load input and ■ for a 77 K load input. The input power P_{in} is calculated from Eq. (10), and $A_{i.f.}$ and $P_{i.f.}$ have been determined with the procedure outlined in Sec. V. The correspondence in bias-voltage dependence between the two sets of curves above the gap voltage is the result of this i.f. calibration. Below the gap voltage a comparable bias-voltage dependence is found for the measured and calculated curves, but the absolute value of the calculated i.f. output power is higher than the measured one.

To match theory and experiment below the gap voltage A_{ex} and P_{ex} are adapted. The curve given in Fig. 7(b) is the result of the subtraction of the measured i.f. output power at the hot and cold input. Assuming that all terms in Eq. (1) except the one with P_{in} do not change for a hot or cold load input, the difference only depends on P_{in}, A_m, and A_{ex}. The curve given by ▲ in Fig. 7(b) is calculated with $A_{ex}=0.43$ resulting in a good match with the experimental curve.

The total i.f. output power P_{out}, calculated with this value for A_{ex}, is given in Fig. 8(a). To obtain these curves, P_{ex} must be chosen equivalent to a blackbody of 49 K. The various contributions to P_{out} as given in Eq. (1) are shown in Fig. 8(b), where the term with P_{ex} is indicated by crosses. Note the bias-voltage dependence of $A_m P_{ex}$, necessary to match theory and data. The value of P_{ex} is 3–4 times as large as the calculated shot-noise contribution P_S (indicated by solid squares). The contribution of the i.f. ($P_{i.f.}$, solid line) and P_S overlap on the first photon step.

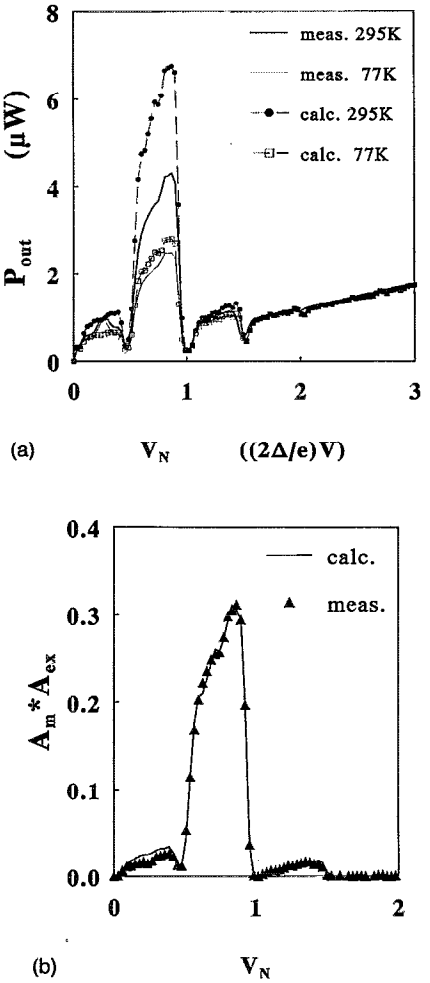

FIG. 7. (a) Measured (continuous lines) and calculated (●, □) i.f. output power for a single-junction mixing element (S44-f1) as a function of bias voltage at a 77 and 295 K input load, respectively. The i.f. output power is given as measured by the power meter. The curves are calculated from Eq. (1) for $P_{ex}=0$ and $A_{ex}=1$. The voltage scale is normalized to the gap voltage $2\Delta/e$. (b) Measured mixer gain (▲) and calculated (solid line) with $A_{ex}=0.43$.

The values for P_{ex} and A_{ex} for 15 different measurements, representing various different bias and tuning conditions, on six different samples are summarized in Table I. For sample S44-f1 the tuning is varied around the optimum tuning point in the mixer block with two tuners (2T). The embedding admittances as determined from the pumped I-V curves, also given in Table I, are normalized to the normal-state conductance of the junction. All points are taken in the sensitive tuning range of the mixer (Sec. IV B). Negative dynamic resistances on the dc I-V curve have been avoided because this detoriates the shape of the i.f. output power as a function of bias voltage.

The values for A_{ex} and P_{ex} appear to be hardly influenced by the change in embedding impedances and the corresponding change in calculated mixer performance.

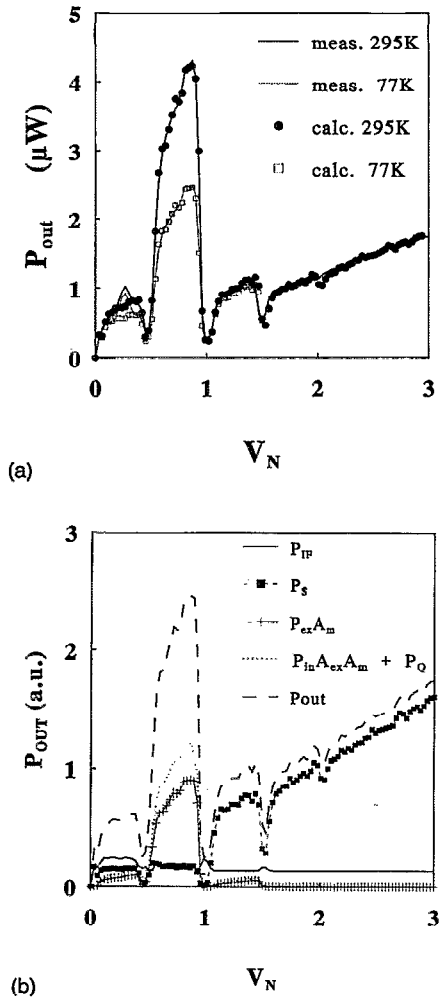

FIG. 8. (a) Same data (solid lines) as in Fig. 7(a), but now the i.f. output power (●,□) is calculated with A_{ex}=0.43 and P_{ex}=49 K. (b) Contributions of the various terms of Eq. (1) to the i.f. output power for a 77 K input load. The contribution of the i.f. stage $P_{i.f.}$, and the shot-noise contribution P_S have the same magnitude over the first photon step.

The calculated mixer gain A_m and mixer shot-noise contribution referred to the input of the mixer are given in Table II. When a 500–50 Ω transformer is used at the i.f. port (entry no. 5) to enhance the coupled mixer gain, a larger gain is indeed observed, while the value of A_{ex} does not change. When the calculated shot-noise contribution is doubled by a different choice of embedding impedances (entry no. 4) the value P_{ex} does not change significantly.

Sample S44-f1 has also been measured in the mixer block with one tuner (1T), since losses in mechanical tuning elements, which are unknown and difficult to measure, are expected to influence A_{ex}. Although the 2T mixer block allows a wider choice in embedding impedances, in this case a comparable embedding impedance is obtained in a mixer block with one tuner (compare, e.g., entries 1 and 3 which are measurd at the same LO power). The value for A_{ex} is indeed higher in the 1T block. Averaged over all measurements, A_{ex} is 0.44 in the 2T mixerblock and 0.55 in the 1T block.

In this comparison measurement no. 6 deserves special

TABLE II. Mixer parameters. The mixer parameters of the measurements in Table I are shown at the optimum bias voltage. A_m is the calculated mixer gain, and A_mA_{ex} is the measured mixer gain. $P_S/(A_mA_{i.f.})$ is the calculated mixer shot-noise contribution, referred to the input of the mixer. A_{ex} and P_{ex} are copied from Table I for ease of reference. P_{sg} is the shot-noise spectral density, in units of K, associated with the subgap current of the unpumped I-V curve, averaged over the bias-voltage region of the first photon step at 350 GHz.

No.	N	A_m	A_mA_{ex}	$P_S/(A_mA_{i.f.})$ (K)	A_{ex}	P_{ex} (K)	P_{sg} ±15 K
1	1	0.7	0.3	15	0.43	49	50
2	1	0.53	0.2	16	0.38	46	50
3	1	0.66	0.23	13	0.35	48	50
4	1	0.45	0.18	27	0.39	51	50
5	1	1.13	0.45	12	0.4	47	50
6	1	3	0.23	15	0.55	63	70
7	2	0.9	0.56	9	0.57	41	40
8	2	0.7	0.35	12	0.5	41	40
9	2	0.76	0.38	16	0.5	62	60
10	2	0.45	0.25	12	0.47	58	60
11	2	0.31	0.18	10	0.61	53	50
12	2	0.36	0.22	11	0.63	53	50
13	2	0.4	0.25	12	0.65	53	50
14	4	0.56	0.26	14	0.48	45	55
15	4	0.5	0.28	14	0.44	45	55

attention since an integrated tuning element in the form of an open-circuited superconducting transmission line stub is added parallel to the junction. This reduces the Q factor of the tuning arrangement considerably, as can be seen from the embedding impedances, and has also been observed from the much less critical positioning of the mechanical tuner. The high mixer gain, resulting from this broadband tuning, complicates the analysis. The measured and calculated i.f. output power are shown in Fig. 9. The values of A_{ex} and P_{ex} are based on a comparison of measurement and calculation on the second quasiparticle step and the onset of the first step. The mixer appears to saturate at the high-gain peak at the first photon step. Although comparison of the curves for only a part of the bias-voltage region is less accurate, it seems that A_{ex} does not change drastically when an integrated tuning element is used. We have not analyzed two or more junctions in series with integrated tuning, because of the problems with saturation. Also a possible imbalance between two junctions together with this type of integrated tuning element complicates the analysis.

At every tuning point the I-V curve and the i.f. output power are measured at several LO power levels. A considerable change in the LO power (entries no. 11–13) does not significantly change the values for A_{ex} and P_{ex}. Figure 10 shows the dc I-V curve and the measured and calculated i.f. output power for low (P1), optimum (P2), and high (P3) LO power. This behavior has been observed up to very low LO powers, where the pump step is hardly visible in the dc I-V curve.

Additionally, by using single-junction mixing elements as well as series arrays it has been tested whether arrays cause excess noise, as has been reported at lower

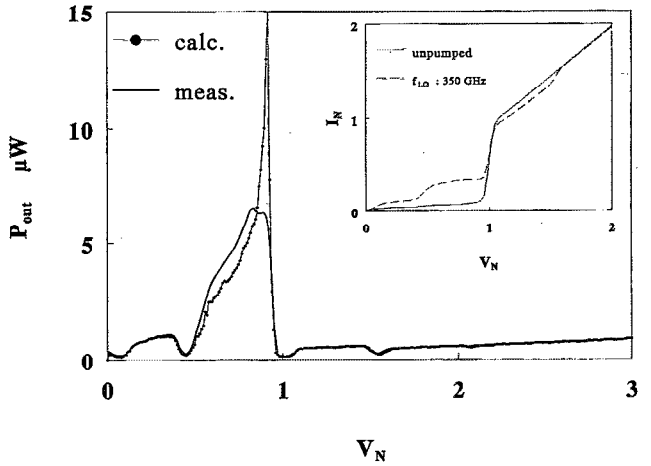

FIG. 9. Measured (thick line) and calculated (line with dots) i.f. output power at a 295 K load input for sample S42-f4 (integrated tuning), with $A_{ex}=0.58$ and $P_{ex}=63$ K. In the inset the associated measured pumped and unpumped I-V curves are shown. The slope of the pumped curve is positive at all bias points.

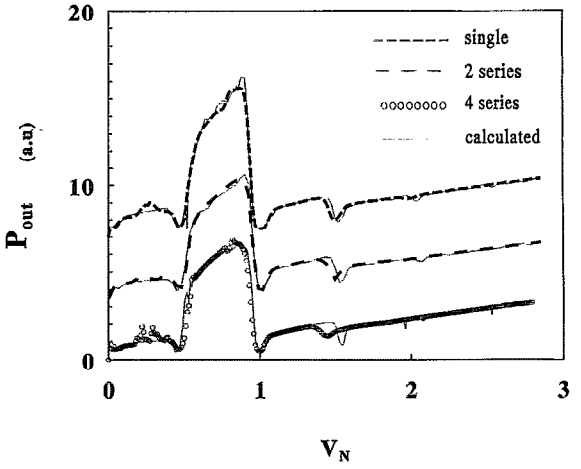

FIG. 11. Measured i.f. output power as a function of bias voltage for a single junction (S44-f1, dashed line) a two-junction array (S44-e11, fine dashed line), and a four-series array (S44-c3, O line), at a 295 K input load. The bias-voltage scale is normalized to $2N\Delta/e$, where N is the number of junctions in series. The calculated curves, for the appropriate values of As A_{ex} and P_{ex}, are given by the thin line and agree well with the measurements. Deviations occur predominantly above the gap voltage.

frequencies.[15] Measured in the same setup, we find no significant difference in P_{ex} or A_{ex}. In Fig. 11 the measured and calculated i.f. power, at an input signal of 295 K, are given for a single-element junction, two in series and four in series. The gap of all three samples is normalized to unity to facilitate comparison. It can clearly be seen that, contrary to the single junction, in the four-junction sample the quasiparticle step above the gap is only weakly present and displaced. Below the gap voltage, the three samples show comparable performance, except for some remnants of the ac Josephson effect.

Finally, when P_{ex} and A_{ex} are determined, the contributions to the total receiver noise temperature T_{rec} can be analyzed. All noise contributions, referred to the entrance of the receiver Dewar, are shown in Fig. 12 as a function of bias voltage. All temperatures are equivalent blackbody temperatures. It can be seen that the contribution of P_{ex}, referred to the receiver input being $P_{ex}/(A_{ex}A_fA_w)$, is the dominant contribution to the receiver noise.

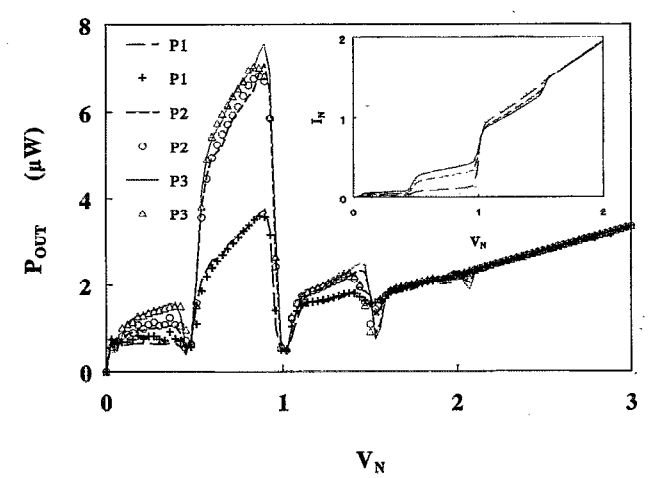

FIG. 10. Measured pumped I-V characteristics (inset) and i.f. output power at three different pump levels at an identical embedding impedance for sample S44-e11. P1:P2:P3 are related as 1:4:6. The calculated i.f. output powers, (P1,+;P2,O;P3,Δ) are given for $A_{ex}=0.63$ and $P_{ex}=53$ K.

VIII. EVALUATION OF THE RESULTS

Evidently Eq. (1) provides a good description of the voltage-dependent response of the mixer. For a perfect

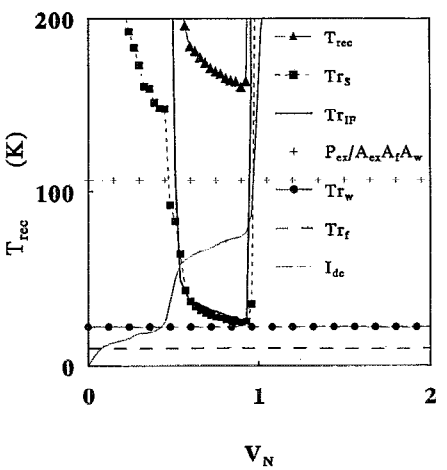

FIG. 12. Contributions to the measured receiver noise temperature of sample S44-f1 T_{rec}, referred to the entrance of the vacuum window of the Dewar. The temperatures are equivalent blackbody temperatures. $T_{r_{i.f.}}$ is the contribution of the i.f. stage, and T_{r_s} is the calculated shot-noise contribution. T_{r_w} and T_{r_f} are the thermal noise contributions of the window and the IR filter at 77 K, respectively. In the calculation we used $A_{ex}=0.43$ and $P_{ex}=49$ K. The figure shows that contribution of P_{ex}, $P_{ex}/(A_{ex}A_wA_f)$, is the largest contribution to T_{rec}. The pumped I-V curve I_{dc} is given for reference.

match between theory and data a loss factor A_{ex} of about 0.5 is introduced as well as an extra intrinsic noise input power P_{ex}, equivalent to a blackbody of about 50 K. To identify possible physical causes for both parameters we performed a number of additional experiments.

A. Accuracy of the parameters used

The accurate determination of P_{in}, $A_{i.f.}$ and $P_{i.f.}$ [Eq. (1)] is crucial to the analysis. The input losses are included by calculating the power incident on the mixer from Eq. (10). The transmission of the beamsplitter, the Dewar window, and the IR filter have been measured separately, at room temperature, in a Michelson interferometer. The inaccuracy in the transmission of the three elements adds approximately 6% to the error in the measured mixer gain ($=A_{ex}$). The gain of the i.f. system is determined *in situ*, including all cable and connector losses. Its contribution to the error in A_{ex} is estimated at 2%. The error margin is small because $A_{i.f.}$ can be checked on the slope of the i.f. output power above the gap voltage. Including also the uncertainty in the physical temperature of the load and the input optics, the error in A_{ex} is estimated to be 10%

The transmission of the cold lens, which contributes to A_{ex}, is also measured at room temperature. The back-to-back transmission of two identical horns plus lenses is 85%. The lens has been positioned on the mixer block at room temperature, using a bismuth bolometer as a detector in the mixerblock. The transmission of the lens at 4.2 K has not been measured. We compared the beam pattern at room temperature and at 4.2 K, to check for deformations of the lens and defocusing. No measurable deviations in coupling to the hot/cold load are found.

Even if A_{ex} can be totally attributed to loss at 4.5 K, it does not affect the analysis of P_{ex}. From Eqs. (1) and (10) it can be seen that the main contribution to the error in P_{ex} comes from the inaccuracy in P_{in} and A_{ex}. The maximum error in the first term of Eq. (1) is 18%, which leads to a maximum error of ± 27 K in P_{ex}. The percentage of error in the i.f. noise temperatures is 10%–15% but due to its low absolute value it hardly contributes to the error in P_{ex}. The measured noise output of an unpumped junction is well described by theory over a full bias range, which indicates that the amplifier operation remains stable both for very high and very low source impedances.

As to the point of the origin of P_{ex} we readdress an issue raised in Sec. III concerning the choice of P_{ex} and A_{ex} in Eq. (1). By replacing P_{ex} by $P'_{ex} = P_{ex}/A_{ex}$ the same equation results; but, P'_{ex} suggests an external source, equivalent to a temperature of about 100 K. Such a high extra input power can only be due to the LO source. A narrow-band (± 500 MHz) Fabry–Pérot filter has been placed between the mixer and the LO source. At the same LO power level on the junction no change in i.f. output noise power is observed. Also, no difference in P_{ex} is observed when the carcinotron is replaced by a solid-state oscillator. This excludes the possibility that P_{ex} is due to the LO source. Hence, we believe that Eq. (1) is the physically correct formulation, indicating that P_{ex} has an intrinsic origin.

All input elements have been replaced, one by one, by equivalent ones of different materials, with slightly different transmissions. The change in the A_{ex} and P_{ex} was well within the error limits mentioned above, typically less than 7% in A_{ex}, and ± 10 K in P_{ex}, which demonstrates the robustness of the analysis to changes in the input optics.

If we replace the beamsplitter ($A_{bs}=89\%$) by one with a transmission of 63%, the signal incident on the mixer at a 77 K input load becomes higher, while the input signal at the 295 K load stays the same. Leaving all mixer parameters constant, the i.f. output has been measured in both cases. The values for A_{ex} and P_{ex} came out exactly the same for both beamsplitters. This rules out an explanation for A_{ex} and P_{ex} based on input saturation.

B. Extension of the theoretical mixer model

It has been argued by Kerr, Pan, and Withington[33] that for ωRC products of 4–10 a five-port mixer model offers a better description of a SIS mixer than a three-port model. In a five-port model, called quasifive port in Ref. 33, the first harmonic signal and image frequencies are not short circuited, but the LO wave form across the junction is still taken as sinusoidal. Adding two ports ($i=2$, $i=-2$) to the mixer model changes the conversion matrix in Eq. (3) to a 5×5 matrix, while the bias conditions of the mixer remain the same. For the embedding impedances at the harmonic frequencies the results from the scale model measurements are used by putting them in parallel to the geometrical capacitance of the junctions. From this analysis we find a negligible change in the calculated gain and noise of the mixer. If we allow some conversion from the harmonic frequencies by changing the embedding impedance at ports 2 and -2, the gain and noise curves change first at the second quasiparticle step below the gap. So, we may have some conversion from the first harmonics but it cannot be used to explain the values for A_{ex} and P_{ex}.

C. Losses in the mixer block

Previously we showed[21] that the embedding impedances obtained from the fitting procedure at 350 GHz agree very well with those found from scale model measurements at 3.3 GHz. Hence, it was argued that the loss in the tuning circuit is less than 1 dB. This seems to be confirmed by the small difference in the value of A_{ex} for different mixer blocks. The removal of one tuner changes A_{ex} from an average of 0.44 to 0.55 (Table I). Changing the Q factor of the tuning considerably by using an integrated tuning element does not change A_{ex} significantly. Different mountings of the same junction lead to slight differences in the position of the junction in the substrate channel; also, the amount of glue may vary. These variations lead to differences of up to 25% in A_{ex}, from 0.45 to 0.58. We never observed in any of the measurements a value for A_{ex} larger than 0.65. Thus, it seems likely that loss in the tuning arrangement contributes to A_{ex}, but is not the dominant contribution.

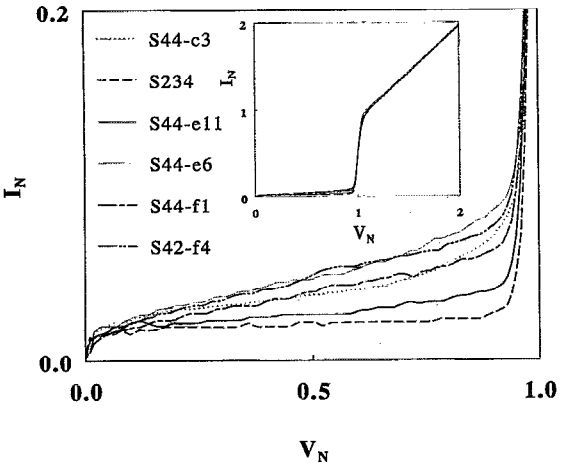

FIG. 13. Unpumped I-V curves on a normalized scale, showing the relative magnitudes of the subgap currents for the samples listed in Table I. All gap voltages are normalized to $2N\Delta/e$, where N is the number of junctions in series. The inset shows the overall shape of the normalized I-V curves.

D. The junction model

The unpumped dc I-V curve of the SIS junction is an important input parameter of the quantum theory of mixing. The applied magnetic field changes the I-V curve. We applied a field strength of two, three, and four fluxquanta per junction area. In the last case the gap is suppressed to 90% of its value at zero field. The pumped I-V curves at higher magnetic fields are very well described by the same equations and embedding impedances as the curves at lower fields, provided that the unpumped input curve is taken at the same higher field. The mixer gain decreases as the magnetic field deforms the I-V curve, but the decrease is well described by the three-port model, provided that the appropriate unpumped I-V curve is used as input parameter. Within the error limits of the analysis the mixer noise does not change when the magnetic field is increased.

In Fig. 13 the unpumped I-V curves of the six studied samples are shown on a normalized voltage and current scale. All samples show some subgap current, and the bias-voltage dependence of those currents is not the same in all samples. In the junction with the lowest subgap current (S234), this current is approximately a factor of 2 higher than the thermal current in an ideal BCS junction. We find (Table I) that P_{ex} is slightly higher (63 and 60 K) for the two samples, S42-f4 and S44-e6, with the highest normalized subgap current. The shot-noise power spectral density P_{sg} corresponding to the subgap current I_{sg} at the dynamical resistance R_{dyn} of the subgap current is of the same order of magnitude as P_{ex}. The value of P_{sg} $(=2eI_{sg}R_{dyn}/N$, where N is the number of junctions in series), averaged over the bias range of the first quasiparticle step, is given in Table II. This interesting correlation between P_{ex} and P_{sg} suggests that a lower value of P_{ex} may be obtained by using junctions with a lower subgap current. At present it is unknown how an increased subgap current affects the noise analysis. If the subgap current is due to imperfections in the barrier, a fundamental assumption in the Tucker theory, first-order elastic tunneling may be violated.

IX. CONCLUSIONS

In this article we have given a full analysis of the performance of two 345 GHz waveguide mixers with Nb-Al_2O_3-Nb SIS junctions as the detector. The results are summarized in Table I and further substantiated by the additional measurements reported in Sec. VIII. They demonstrate that the three-port approximation of the quantum theory of mixing predicts the dependence of mixer performance at 350 GHz on all tested mixer parameters very well. No major discrepancies have been identified for variations in mixing elements, bias conditions, tuning arrangement, and magnetic-field strength. Single-junction mixer elements and arrays of two and four junctions in series have been tested under identical circumstances. No difference in mixer gain and noise is found between these samples in the stable bias range. Only above the gap voltage do arrays of junctions in series deviate at a lower bias voltage from the theoretically predicted behavior for single junctions, probably because of nonequilibrium effects (heating).

We have demonstrated that an additional loss factor A_{ex} and an additional contribution to the intrinsic mixer noise P_{ex} must be added to all measurements, to obtain a perfect match between theory and data. A_{ex} and P_{ex} are independent of the embedding impedance, the LO power, and the number of junctions in a series array. A_{ex} ranges from 0.35 to 0.65, and P_{ex} from 41 to 63 K. P_{ex} is regarded as an intrinsic noise contribution after having excluded a number of possible external sources. We are intrigued by the fact that despite the many variations we have employed A_{ex} and P_{ex} always end up around 0.5 and 50 K, respectively.

A_{ex} is weakly dependent on the mixer block, indicating that part of A_{ex} is due to losses in the tuners. Irreproducability in the mounting of the junction is reflected in A_{ex}, indicating that the performance of the rf filter in the substrate channel is critical to mounting. The application of integrated tuning has only a small effect on A_{ex}. The maximum value observed for A_{ex} is 0.65, which leaves an unexplained power loss of 35% at 4.5 K.

The difference between the calculated and the measured mixer noise contribution P_{ex} is about three times as large as the theoretical mixer noise and dominates the receiver noise. P_{ex} is independent of accidental variations in positioning the junction confirming the assumption that P_{ex} is intrinsic. P_{ex} appears to be dependent on the subgap current, indicating that a more subtle physical model for the junction may be needed. A possible relation between P_{ex} and A_{ex} cannot be ruled out.

ACKNOWLEDGMENTS

We thank A. Skalare and J. van der Kuur for helpful discussions, R. A. Panhuyzen for the realization of the masks, and H. van der Stadt for constant support. This

work is supported by the European Space Agency (ESA) under Contract No. 7898/88/NL/PB(SC) and by the Nederlandse Organisatie voor Wetenschappelijk Onderzoek (NWO) through the Stichting voor Technische Wetenschappen (STW) and the Stichting voor Fundamenteel Onderzoek der Materie (FOM).

[1] B. N. Ellison, P. L. Schaffer, W. Schaal, D. Vail, and R. E. Miller, Int. J. Infrared Millimeter Waves **10**, 937 (1989).
[2] E. C. Sutton, W. C. Danchi, P. A. Jaminet, and R. H. Ono, Int. J. Infrared Millimeter Waves **11**, 133 (1990).
[3] H. Rothermel, D. Billon-Pierron, and K. H. Gundlach, in Conference Digest of the 16th International Conference on Infrared Millimeter Waves, 1991, p. 135.
[4] A. Karpov, M. Carter, B. Lazareff, D. Billon-Pierron, and K. H. Gundlach, in Proceedings of the Third International Symposium on Space Terahertz Technology, 1992, p. 244.
[5] C. K. Walker, J. W. Kooi, M. Chant, H. G. LeDuc, P. L. Schaffer, J. E. Carlstrom, and T. G. Phillips, Int. J. Infrared Millimeter Waves **13**, 785 (1992).
[6] G. de Lange, C. E. Honingh, M. M. T. M. Dierichs, H. H. A. Schaeffer, R. A. Panhuyzen, T. M. Klapwijk, H. van der Stadt, and M. W. M. de Graauw, IEEE Trans. Appl. Supercond. (to be published).
[7] T. H. Büttgenbach, R. E. Miller, M. J. Wengler, D. M. Watson, and T. G. Phillips, IEEE Trans. Microwave Theory Tech. **MTT-36**, 1720 (1988).
[8] A. V. Räisänen, W. R. McGrath, P. L. Richards, and F. L. Lloyd, IEEE Trans. Microwave Theory Tech. **MTT-33**, 1495 (1985).
[9] S.-K. Pan, A. R. Kerr, M. J. Feldman, A. W. Kleinsasser, J. W. Stasiak, R. L. Sandstrom, and W. L. Gallagher, IEEE Trans. Microwave Theory Tech. **37**, 580 (1989).
[10] S. V. Shitov, V. P. Koshelets, S. A. Kovtonyuk, An. B. Ermakov, N. D. Whyborn, and C. O. Lindström, Supercond. Sci. Technol. **4**, 406 (1991).
[11] A. Skalare, H. van der Stadt, Th. de Graauw, R. A. Panhuyzen, and M. M. T. M. Dierichs, in Proceedings of the Third International Symposium on Space Terahertz Technology, 1992, p. 222.
[12] V. Yu. Belitsky, M. A. Tarasov, S. A. Kovtonjuk, L. V. Fiilipenko, and O. V. Kaplunenko, Int. J. Infrared Millimeter Waves **13**, 389 (1992).
[13] Th. H. Büttgenbach, H. G. LeDuc, P. D. Maker, and T. G. Phillips (unpublished).
[14] J. R. Tucker and M. J. Feldman, Rev. Modern Phys. **57**, 1055 (1985).
[15] W. R. McGrath, P. L. Richards, D. W. Face, D. E. Prober, and F. L. Lloyd, J. Appl. Phys. **63**, 2479 (1988).
[16] C. A. Mears, Q. Hu, P. L. Richards, A. H. Worsham, D. E. Prober, and A. V. Räisänen, IEEE Trans. Magn. **MAG-27**, 3363 (1991).
[17] M. J. Feldman, S.-K. Pan, A. R. Kerr, and A. Davidson, IEEE Trans. Magn. **MAG-19**, 494 (1983).
[18] P. L. Richards, T.-M. Shen, R. E. Harris, and F. L. Lloyd, Appl. Phys. Lett. **34**, 345 (1981).
[19] S. Rudner, M. J. Feldman, E. Kollberg, and T. Claeson, J. Appl. Phys. **52**, 6366 (1981).
[20] D. W. Crété, W. R. McGrath, P. L. Richards, and F. L. LLoyd, IEEE Trans. Microwave Theory Tech. **MTT-35**, 435 (1987).
[21] C. E. Honingh, G. de Lange, M. M. T. M. Dierichs, H. H. A. Schaeffer, Th. de Graauw, and T. M. Klapwijk, IEEE Trans. Microwave Theory Tech. (to be published).
[22] A. W. Love, Microwave J. **5**, 117 (1962).
[23] M. Carter (personal communication).
[24] J. F. Johansson and N. D. Whyborn, IEEE Trans. Microwave Theory Tech. **MTT-40**, 795 (1992).
[25] C. E. Honingh, H. H. A. Schaeffer, Th. de Graauw, M. M. T. M. Dierichs, and T. M. Klapwijk, in Proceedings of the Second International Symposium on Space Terahertz Technology, 1991, p. 473.
[26] M. J. Feldman and S. Rudner, Rev. Infrared Millimeter Waves **1**, 47 (1983).
[27] A. R. Kerr, IEEE Trans. Microwave Theory Tech. **MTT-27**, 938 (1979).
[28] M. J. Wengler and D. P. Woody, IEEE J. Quantum Electron. **QE-23**, 613 (1987).
[29] A. Skalare, Int. J. Infrared Millimeter Waves **10**, 1339 (1989).
[30] J. R. Tucker, IEEE J. Quantum Electron. **QE-15**, 1234 (1979).
[31] M. Gurvitch, M. A. Washington, and H. A. Huggins, Appl. Phys. Lett. **42**, 472 (1983).
[32] M. M. T. M. Dierichs, R. A. Panhuyzen, C. E. Honingh, M. J. de Boer, and T. M. Klapwijk, Appl. Phys. Lett. **62**, 774 (1993).
[33] A. R. Kerr, S.-K. Pan, and S. Withington, IEEE Trans. Microwave Theory Tech. (to be published).